Vacuum 192 (2021) 110482

Contents lists available at ScienceDirect

Vacuum

journal homepage: www.elsevier.com/locate/vacuum

Wear in hard metal check valves: In-situ surface modification through tribolayer formation in dry contact

A. Blutmager [a], M. Varga [b,*], U. Cihak-Bayr [b], W. Friesenbichler [c], P.H. Mayrhofer [d,**]

[a] Wittmann Battenfeld GmbH, A-2542, Kottingbrunn, Austria
[b] AC2T research GmbH, Viktor-Kaplan-Straße 2/C, 2700, Wiener Neustadt, Austria
[c] Chair of Injection Moulding of Polymers, Department Polymer Engineering and Science, Montanuniversität Leoben, Otto-Glöckel Str. 2, 8700, Leoben, Austria
[d] Institute of Materials Science and Technology, TU Wien, A-1060, Vienna, Austria

ARTICLE INFO

Keywords:
Injection moulding
Check valve
Tribology
Material transfer
Hard metal
Tribolayer

ABSTRACT

Tools in injection moulding units, especially the check valves, can suffer dry hard metal - hard metal contact under severe conditions, thus experiencing increased wear. For the present study, various hard metal pairings were investigated using dry pin-on-disc tests to simulate the tribosystem of the check valve. Hard metal discs with W_xC particle sizes between ~0.9 and 3 μm and binder contents between 9 and 17.5 wt. %, were tested against similar pins with smaller W_xC particles. Results show that the cracking of carbides is the major wear mechanisms and that decreased W_xC particles sizes together with decreased binder contents lead to lower wear rates. The combination of the hard metal with the smallest W_xC particles and the lowest hardness differences between pin and disc leads in this case to a beneficial material transfer and tribolayer formation, resulting in increased wear resistance of both sliding counterparts, promising a lifetime enhancement of the check valves.

1. Introduction

1.1. Application: check valve in injection moulding

Injection moulding is a plastic processing technology with the best performance ratio between material input and output. An overview on the plasticisation process and involved temperature and pressure distribution can be found in [1] which also vary with machine types [2]. Wear of machine components is an important issue during injection moulding. Wear phenomena change during the course of the polymer through the plasticising unit: while in the feeding and compression zone wear is dominated by the solid resin contact [3], leading to abrasive wear phenomena - especially when filled polymers are processed - the wear in the metering zone and subsequent mould is dominated by the flow of the polymer melt [4,5] and erosive phenomena [6]. Wear in the check valve differs therefrom.

The check valve is one of the essential components that determine the reproducibility and thus the efficiency of the injection moulding process. When the check valve is closed, it prevents the backflow of the plasticised mass during the injection (the shut-off ring closes with contact to the check ring by pressure from left in Fig. 1). During dosing, the valve is open (pressure from right in Fig. 1), so that the mass can flow through the shut-off ring and between the flights entailing the before mentioned erosive wear phenomena. A second, much more severe wear mechanism can occur on the check valve when a dry contact between the flights and the shut-off ring takes place. This appears when poorly lubricating plastics are processed or when plastics are processed at very high dosing speeds (rotation of the dosing screw and check valve tip) leading to high relative movement between these two valve components (the shut-off ring is dragged by the plastic mould and thus has lower circumferential speed than the tip), as this can lead to a failure of the separating plastic mould film [7,8].

Nominal contact pressures of the check valve during dry contact are calculated to be ~10 MPa for typical processes [9,10]. Circumferential speeds of the check valve are up to ~1 m/s, which is also the maximum possible velocity difference between flights and shut-off ring [9]. Actual relative speeds are highly dependent on specific viscosity and lubricity of the processed polymer and the specific step of the injection moulding process [10].

* Corresponding author.
** Corresponding author.
E-mail addresses: markus.varga@ac2t.at (M. Varga), paul.mayrhofer@tuwien.ac.at (P.H. Mayrhofer).

https://doi.org/10.1016/j.vacuum.2021.110482
Received 8 April 2021; Received in revised form 21 June 2021; Accepted 19 July 2021
Available online 21 July 2021

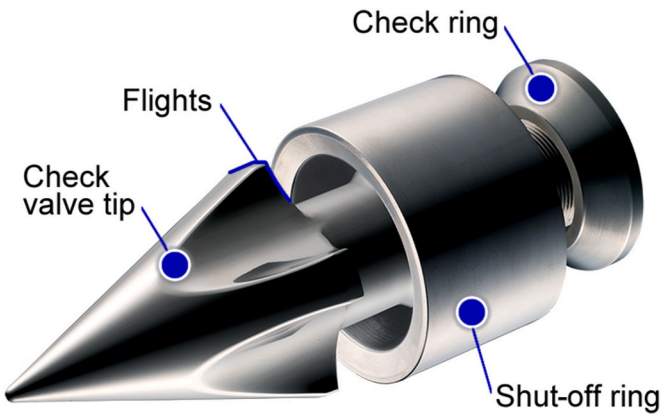

Fig. 1. *Application: Check valve with main components.* [4].

1.2. Sliding wear of hard metals

Cemented carbides, also known as hard metals, are useable for a lot of industrial applications, such as cutting and moulding tools, as well as for wear resistant check valves. Hard metal as wear resistant material developed as an alternative for diamond, combining excellent wear-resistance and chemical-stability, simultaneously allowing for even higher application temperatures. The most common application of hard metals is in the field of cutting tools, which is well characterised, e.g. [11,12,13,14], for shaping of hard metals a few studies are available e.g. [15,16], However, their use in check valve application results in completely different contact conditions than those found in tooling or grinding applications. The counterbody is softer in tooling, while for check valves both partners are made of hard metal. Additionally, the check valve operation takes place at high temperatures permanently. The operability of the check valve has to be assured for many hundred-thousand injection cycles, which equals to a lifetime of several months. To advantage, wear depths up to a millimetre are tolerable for some plastics before maintenance is required [10,17,18,19]. Generally, sliding hard metal - hard metal contacts have received little attention in the available literature, one of the rare examples is given in [18].

The properties of hard metals (especially rupture strength and wear resistance) are well-known to be dependent on processing parameters, microstructure and also the compatibility between the metallic binder (typically Co) and W_xC particles [20]. In general, wear loss increases with increasing Co content, increasing W_xC particle size and decreasing hardness [21–24]. However, the hardness and binder content are not sufficient to predict the wear resistance of hard metals, especially under dry contact conditions against carbon steel [21,22,25]. The prevalent wear mechanisms include adhesion, abrasion, surface fatigue, or tribochemical reactions [26]. Cemented carbides are affected by the sliding velocities and loading conditions, as these determine frictional temperatures, which in turn, can promote thermal softening of the binder phase. But also other effects, like particle shape and distribution [27], surface polishing of W_xC particles, (micro-) abrasion, creation of wear debris, formation of tribofilms, binder removal, W_xC particle cracking, and particle shape, play a role with regard to their wear behaviour [28,29,30].

The wear behaviour of hard metals and metal-matrix composites (MMC) is substantially determined by the mechanical support of the hard phases by the metal matrix (i.e., binder phase in hard metals). For example, when used at higher temperatures, the pronounced softening effect experienced by the binder is responsible for decreasing support of the W_xC entailing cracking of the hard particles during loading [31,32,33]. However, wear debris or oxide particles can easily be incorporated into the sliding substrate, leading to the formation of mechanically mixed layers (MML) [34,35]: The debris is embedded into the binder/matrix phase by mechanical mixing. Due to the small size of the wear particles and enhanced temperatures oxidation often plays a major role. MML formation is also well known in abrasive contact with the incorporation of 3rd bodies [36,37]. Further, many metal-oxides (and abrasives) show high hardness and wear resistance, thus locally increasing the wear resistance of the compound. Such layers can provide an effective wear protection under certain conditions [30,38,39,40]. In the field of hard metals tribolayer formation of dry contacts – without 3rd body – is sparsely investigated in the available literature. First evidence was found by Murray and Lewis in 1958 [41]. Engqvist et al. [30] made an analysis of influencing factors in hard metal - hard metal contact, pointing out that high loads are required for effective tribolayer formation, and oxidation plays a major role therein. A recent paper of Chen et al. [42] reports a beneficial tribolayer formation on hard metal as well. They compared WC-17Co produced by different processing routes in dry sliding experiments. Although all materials featured the same chemical composition the different processing leads to different microstructures, wherefrom just one was able to form an effective tribolayer in the tribotest. Obviously, a narrow range determines the ability for beneficial tribolayer formation on hard metals.

To investigate the suitability of various hard metals for check valves in plastic injection moulding applications, the impact of several hard metal characteristics on the wear behaviour during dry sliding experiments has been studied. Three different hard metal pairings were investigated using pin-on-disc tribotests with testing parameters chosen to closely resemble check valve dry sliding conditions occurring during injection moulding. The major wear mechanisms and their correlation with hard metal properties were identified in the course of a detailed investigation of the worn parts by profilometry, light optical and scanning electron microscopy. A special focus was laid onto the investigation and effectiveness of built tribolayers to protect against wear.

2. Experimental

2.1. Materials investigated

Three representative hard metal pairings, from different suppliers, used in real check valve production, were chosen for this study – the pairings will be referred to as Pairing I, II, and III. In the industrial use two different hard metals are employed to ensure that the shut-off ring (the easier exchangeable part) is worn first. That is reached by significantly harder hard metals for the flights by finer grained W_xC and lower binder content. The shut-off ring is represented by the disc in the model tests and the flights by the pins. In this study, the pins have the prefixes “P” and the discs “D”. The discs were sintered in the size of ø60 × 5 mm and the pins ø4 × 15 mm. The chemical compositions of the hard metals are given in Table 1, where W_xC indicates both tungsten carbide types, WC and W_2C. Most of the materials are Co-bound, while one pin (PII) has a Ni-binder, in order to be able to detect material transfer in subsequent analyses. The binder content is always lower for the pins compared to the discs. Microstructural analyses were carried out by scanning electron microscopy (SEM) on cross-sections. Quantitative image analysis with QWIN® software was done on the SEM images in order to determine

Table 1
Chemical composition, density (according to datasheets) and hardness of hard metal samples.

	W_xC [wt. %]	Co [wt. %]	Ni [wt. %]	Other [wt. %]	Density [kg dm^{-3}]	Hardness [HV10]	[HV30]
DI	86.5	13.5	–	–	14.1	1005 ± 15	1001 ± 27
PI	91.0	9.0	–	–	14.6	1369 ± 36	1370 ± 25
DII	88.0	12.0	–	–	14.3	1160 ± 37	1135 ± 26
PII	88.7	–	10.5	0.8	14.4	1381 ± 70	1369 ± 14
DIII	80.3	17.5	–	2.2	13.6	1182 ± 12	1180 ± 19
PIII	87.9	12.0	–	0.1	14.3	1371 ± 21	1349 ± 12

mean particle sizes and distances. The hardness of the materials was measured with standard Vickers tests using a load of 98.1 N (HV10) and 294.3 N (HV30).

2.2. Dry sliding tests

Dry sliding pin-on-disc tests were performed to simulate the condition in the check valve when the lubricating plastic film fails to separate the flights from the shut-off ring. Thereto a special 3-pin-on-disc setup was utilised (Fig. 2a): three pins are pressed with constant force onto a rotating disc.

Thereby the performance of different hard metal pairings can be studied in application-near conditions, where the shut-off ring is represented by the disc and the flights by the pins. The test parameters were chosen in order to simulate typical check valve operating conditions (see Section 1.1): The 3 pins, each with a diameter of 4 mm, were loaded with 400 N applied total force, resulting in 10.6 MPa nominal contact pressure at each pin – which is close to typical nominal pressures reported for check valves [9]. The chosen sliding speed of 590 mm/s is a typical value in the injection moulding process. The samples were not heated externally, as the frictional heating due to sliding alone led to temperatures above 150 °C, which is a typical value found during injection moulding processes of plastics [9]. Prior studies showed that a testing time of 6 h was sufficient to ensure steady-state conditions. The test parameters are summarised in Table 2.

All tests were repeated 3 times for statistical reliability of the results (i.e., 3 discs and 9 pins). All tested samples were ground to the same surface roughness of Sa = 0.2 µm, to ensure comparable micro-geometrical conditions. The wear resistance of the individual hard metals was quantified by

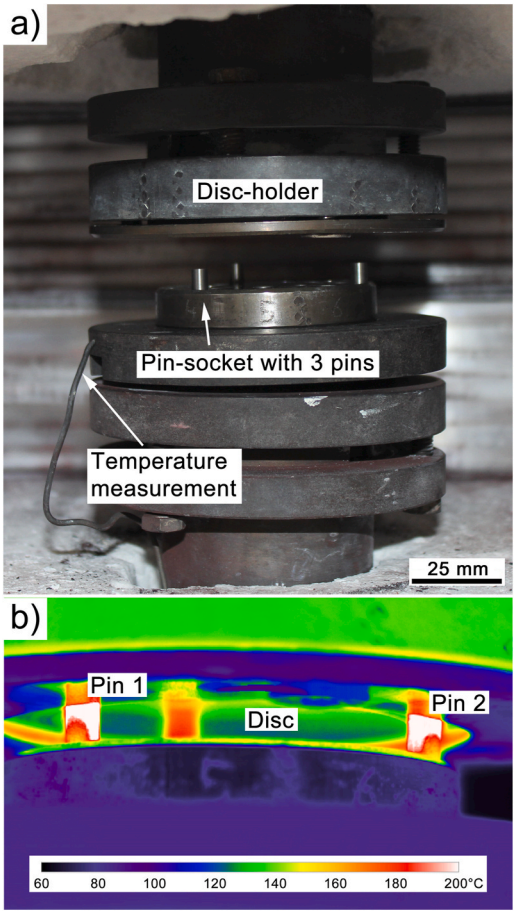

Fig. 2. High temperature 3-pin-on-disc test: a) sample chamber; b) thermography during the final stage of a test.

Table 2
Pin-on-disc test parameters.

Parameters	Value
Pin diameter	4 mm
Disc diameter	60 mm
Mean wear track diameter	47 mm
Mean sliding speed	590 mm/s
Load	400 N/3 Pins
Nominal contact pressure	10.6 MPa
Duration	6 h
Initial roughness Sa	0.2 µm
Wear quantification	Weight loss → Wear rate [$mm^3\ N^{-1}\ m^{-1}$]

their mass loss and the corresponding volume loss was calculated using the density of the materials (Table 1) according to available material datasheets. Wear results are given as the sum of the wear volumes of all three pins or of the disc, divided by the applied force (400 N) and total sliding distance (17,280 m), i.e., as wear rate in $mm^3\ N^{-1}\ m^{-1}$.

The coefficient of friction (CoF) and the temperature of the pin, measured about 10 mm beneath the contact surface (see Fig. 2a), are monitored continuously throughout the experiments [cf. 43]. Thermography of selected tests with a FLIR®C7600 MB infrared camera with InSb-detector provided some insight into the temperature distribution. A typical distribution by the end of the 6 h test run is shown in Fig. 2b, where the pins have clearly heated up by frictional heating. After testing, the wear tracks were analysed with a stereo microscope and SEM, including SEM of representative cross-sections. Wear scar topographies were measured with an Alicona® InfinitFocus G5 system.

3. Results and discussion

3.1. Materials

The microstructures of the hard metals are given in Fig. 3 as acquired by SEM using back scattered electron (BSE) mode to visualize the chemical differences between the W_xC particles and the binder phase. The hard metal pairings I-III are sorted in descending order according to their W_xC particle sizes in the disc samples. The direct comparison clearly shows that the microstructure of the harder pin was significantly finer-grained than those of the softer discs.

Particle sizes (Fig. 4a) and particle distances (Fig. 4b) within the individual hard materials were determined via quantitative image analysis with QWIN® software on SEM images as this is known to influence the wear behaviour [27]. The mean particle sizes of the hard metals (HM) used for the discs are 3.0 ± 1.8 µm, 2.0 ± 1.1 µm, and 0.9 ± 0.5 µm, for DI, DII, and DIII, respectively, while the corresponding pins have mean particle sizes of 1.0 ± 0.7 µm (PI), 0.6 ± 0.3 µm (PII), and 0.6 ± 0.3 µm (PIII). This showed that hardness clearly increased with decreasing particle sizes. The most frequent distance between particles was 0.4 µm (comprising 30% of all distances) for all pin materials, as well as disc material DIII (see Fig. 4b). DII also had a maximum at 0.4 µm, but the distribution of particles sizes was much broader than for the other materials with the same peak position. The DI particle distance distribution was also broader, but here the peak maximum is at 3.5 µm. The larger grain sizes of DII and DI clearly change the particles distance distributions compared to the other samples.

The hardness values listed in Table 1 were measured with standard Vickers tests using a load of 98.1 N (HV10) and 294.3 N (HV30). The high applied loads allowed to obtain averaged values across large areas of the microstructure (including several W_xC carbides and the binder phase). The hardness values of the three pins are similar for the three tested check-valve pairings, while the disc hardness values differ over larger ranges of up to ~180 HV. The hardness differences between disc and corresponding pin are ~370 HV30 for Pairing I, ~235 HV30 for Pairing II, and ~170 HV30 for Pairing III.

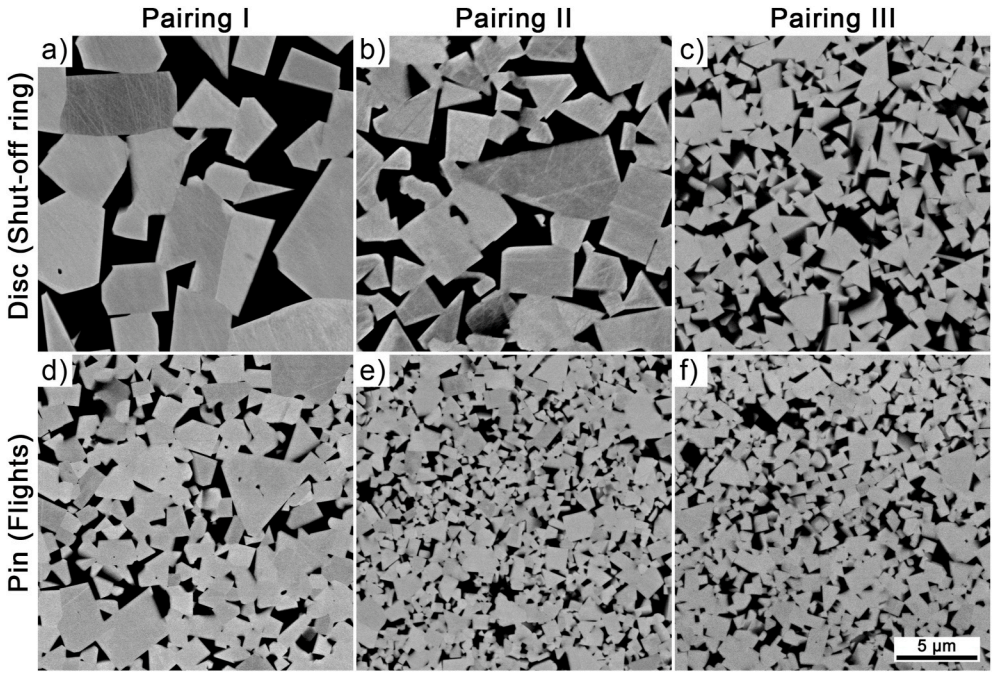

Fig. 3. SEM-BSE images of polished hard metals showing the W_xC appearing bright and the matrix in black. The upper row shows the hard materials used for the discs: a) DI, b) DII, c) DIII, and the lower row shows the hard materials used for the pins: d) PI, e) PII, f) PIII.

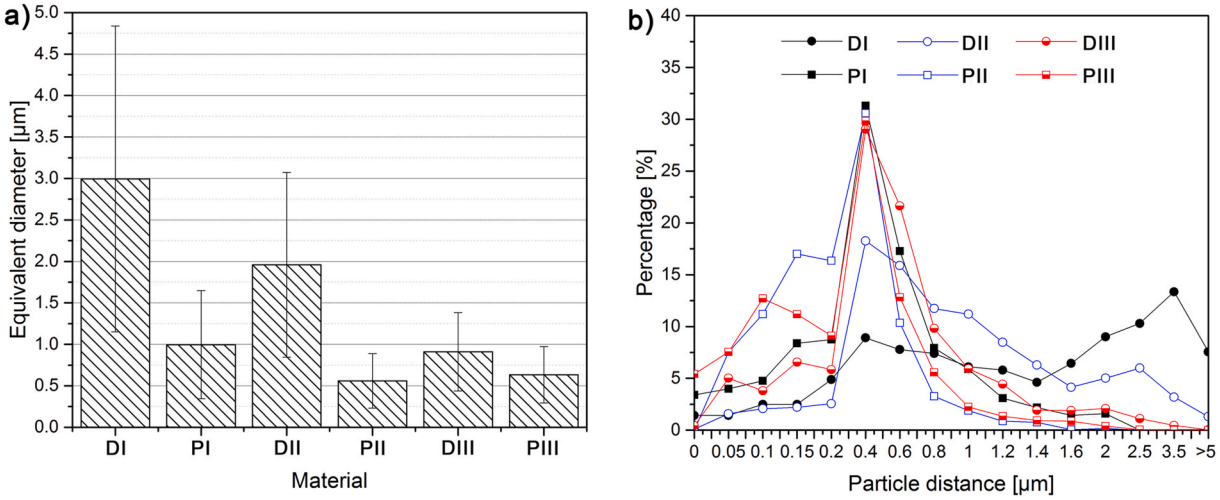

Fig. 4. Particle analysis of the materials investigated: a) average equivalent diameter (calculated from an SEM-BSE image, error bars represent standard deviations), b) histogram of individual particle distances.

3.2. Quantitative wear results

The wear rates, i.e. the wear volume per load and sliding distance, of pins and discs are presented for each pairing in Fig. 5. The wear rates are averaged over three test runs and the corresponding error bars show their standard deviation. For better visibility in the graphs, the wear rates of the discs and pins are scaled differently with a factor of 10 between them. Among the disc samples, DI had the highest wear rate with 1.65×10^{-4} mm^3 N^{-1} m^{-1}, followed by DII with 1.13×10^{-4} mm^3 N^{-1} m^{-1}, while DIII had the lowest wear rate at 0.21×10^{-4} mm^3 N^{-1} m^{-1}. Thus, the wear rate of the discs significantly reduces with decreasing particle sizes – and thereby increasing hardness – of the discs. Even though the discs were tested against different pin counterparts, the material characteristics of the pins were very similar (Table 1) and Fig. 4, showing similar hardness values as well as distributions of particle sizes and particle distances for the individual pins and the differences in disc wear rates can primarily be attributed to the microstructure and hardness of the discs.

When comparing the wear rates of the pins, the above-mentioned differences in the disc microstructures have to be taken into account. The wear rate of PI (3×10^{-6} mm^3 N^{-1} m^{-1}) was not the highest of the individual pins, although this hard metal had the largest mean particle sizes and lowest hardness among the individual pins tested. The moderate wear of PI was attributed to the significantly softer disc counterpart (1001 ± 27 HV30) compared to the other discs which are significantly harder (1135 ± 26 and 1180 ± 19 HV30). PII showed the lowest wear rate and PIII by far the highest, although tested against discs with similar hardness. To study this behaviour the tribosystem was analysed in more detail in the following sections.

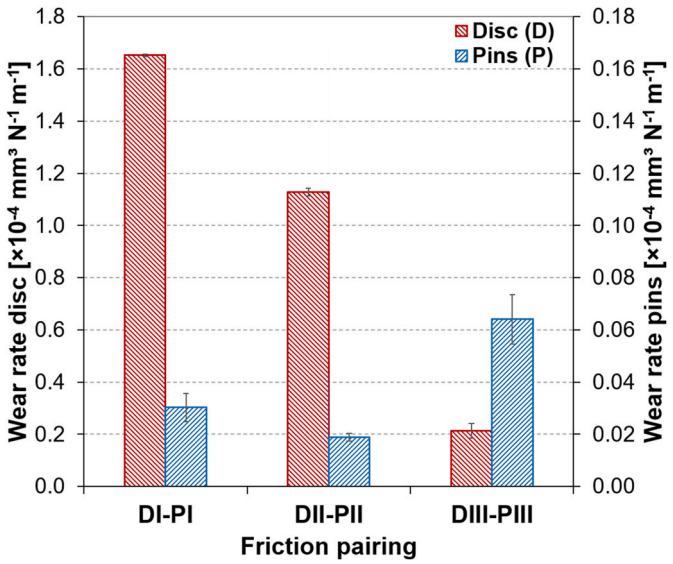

Fig. 5. Wear rates of the hard metal pairings DI-PI, DII-PII and DIII-PIII based on three test repetitions each.

3.3. Friction and temperature evolution

The temperature of the dry tribocontact rapidly increased due to frictional heating, although no external heating was used in the test. For example, the temperatures of the pins determined by a thermo-camera (close to the contact points with the counterbody) increased to 250 °C during the 6 h experiment, which is well beyond the observed sample holder temperature of ~140 °C (Fig. 2b). The temperature profile measured by thermocouples, fixed to the pin-holder, showed slightly lower maximum temperatures, due to individual positioning and thermal conductivity of the sample holder. After an initial steep, but steady increase, the temperature values measured in the pin holder reached about 180–190 °C for most of the test duration, and do not show significant difference between the various material pairings.

The friction-curves (Fig. 6) of the three pairings exhibit two ranges: In the starting period until ~1.5–2 h values fluctuated with high frequency and amplitude, which is regarded as running-in. Afterwards, the CoF fluctuated at a much lower frequency. This running-in period was most pronounced for Pairing II, showing also a steep increase in CoF after this period. The highest CoF values in the steady-state region were obtained for Pairing I (Fig. 6a), which combined the hard metals with the largest W_xC grains and widest particle size distributions among the disc and pin materials. After an estimated running-in period of ~1.5 h, the CoF stabilised between 0.6 and 0.7. Pairing II (Fig. 6b) showed a running-in period with a lower CoF until ~1.5 h. Thereafter the mean value of the CoF reached ~0.6. The average values after a period of 2.5–3 h were close to 0.6, slightly below those of Pairing I. Pairing III (Fig. 6c) showed a running-in period of ~2 h followed by a CoF of ~0.6. In contrast to Pairing II, Pairing III shows short time minima with lower CoF values below 0.5 during the condition regarded as steady-state – an indication of beneficial tribolayers.

3.4. Tribolayer & surface morphology

To investigate the reasons for these different friction and wear results of the studied material pairings, SEM analysis was performed. The SEM results are shown in Fig. 7 - Fig. 9 for the individual pairings. All surfaces exhibit a patchy structure of bright and dark areas in the SEM-BSE images, indicating different chemical composition. The large grained disc samples, DI and DII, were covered by large patches (>50 μm in the sliding direction), which were chemically different from the disc base

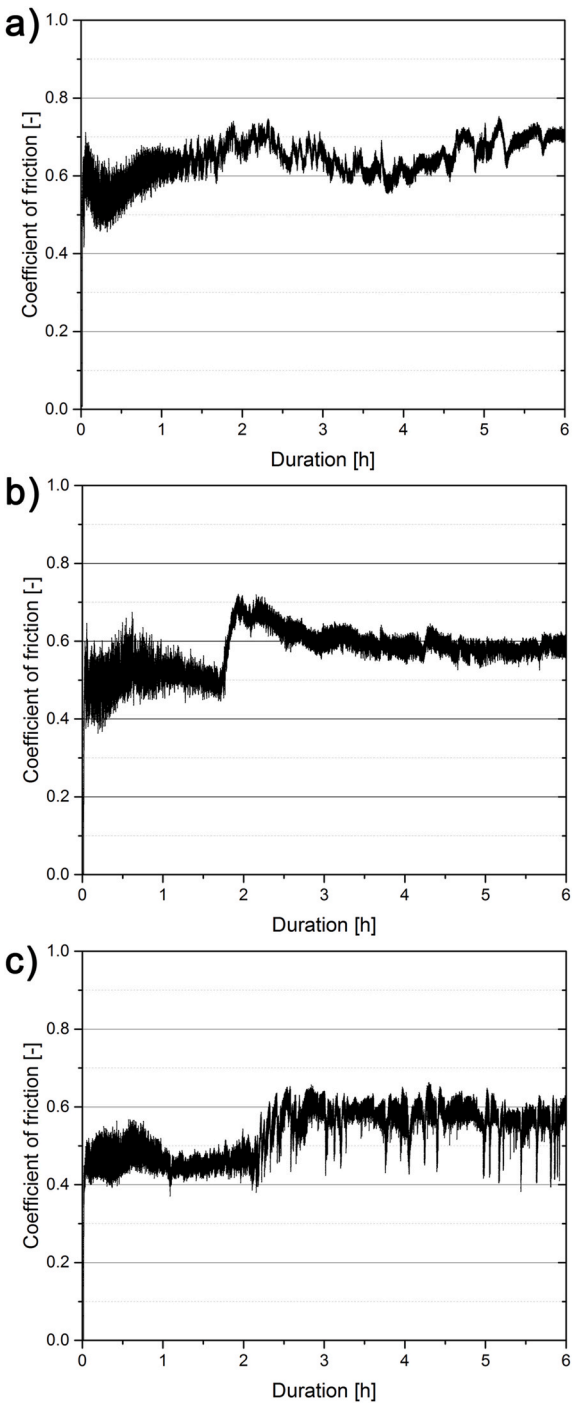

Fig. 6. Exemplary data records of the coefficient of friction as a function of time: a) pairing I, b) pairing II, c) pairing III.

material: the bright patches corresponded to W_xC, the grey zones were enriched with the binder phase, while the dark grey zones exhibit a significant amount of oxides (see EDX position 2 in Fig. 8a, Table 3). Larger magnifications revealed tiny oxides and fragmented carbides that were completely embedded in the soft, oxidised binder phase (darker regions). In these patches, oxidised binder and fragmented W_xC particles were homogenously mixed and are therefore addressed as tribolayers or MMLs.

The tribolayers formed on each individual pairing vary in morphology and thickness, as seen in the cross-sections (Fig. 7b–9b). For Pairings I and II, the layers were ~10 μm thick with a coarse microstructure due to the large broken W_xC particles. For Pairing III, a double

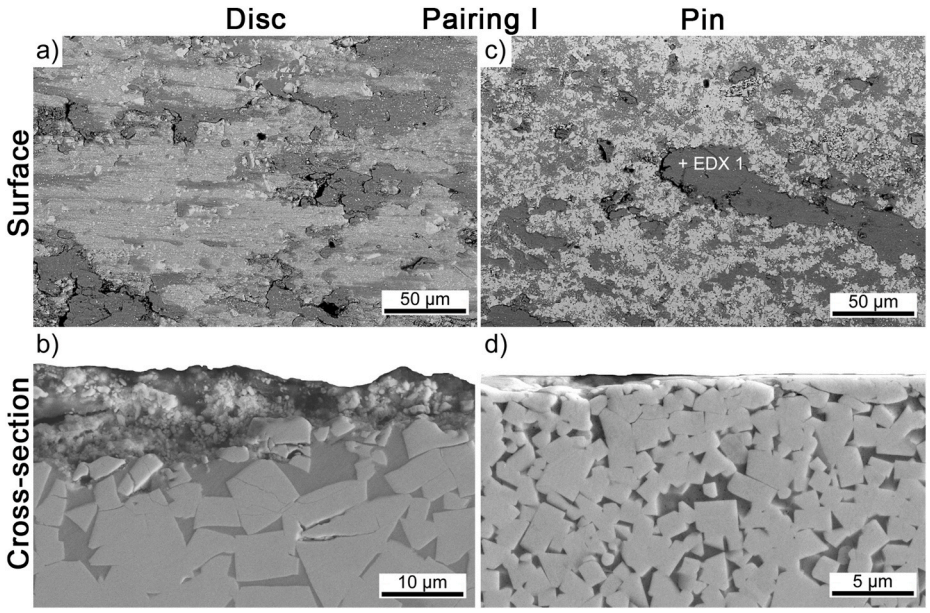

Fig. 7. SEM imaging of Pairing I: a) surface SEM-BSE of disc, b) cross-section SEM - SE of disc, c) surface SEM-BSE of pin, d) cross-section SEM-BSE of pin.

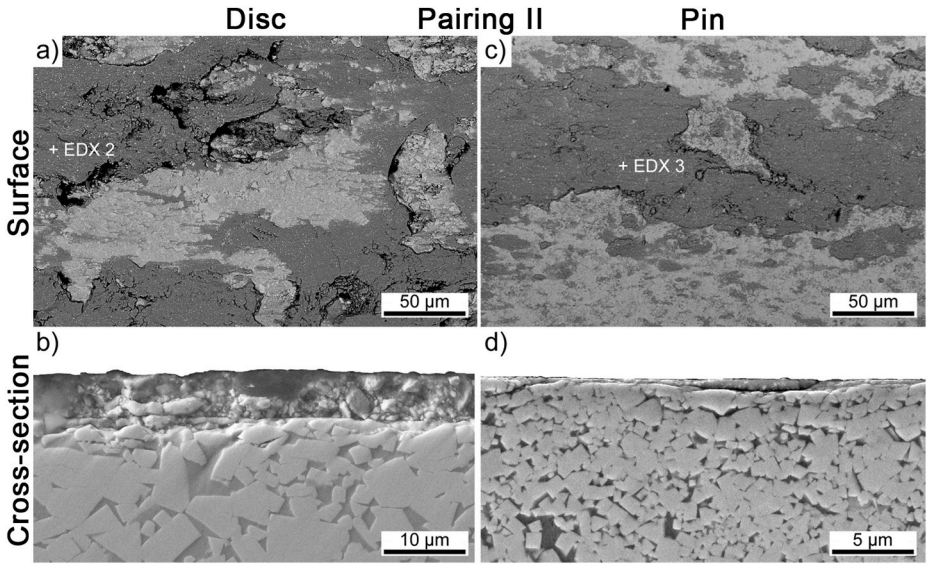

Fig. 8. SEM imaging of Pairing II: a) surface SEM-BSE of disc, b) cross-section SEM - SE of disc, c) surface SEM-BSE of pin, d) cross-section SEM-BSE of pin.

layer is formed, for which the top layer was ~2 µm thin and had a coarse microstructure similar to the layers observed for Pairings I and II. The layer underneath this part is ~3 µm thin and contained higher Co- and lower W-amounts (compare EDX 4 with EDX 5 in Table 3). The W signal is most likely increased by the W_xC beneath the layer, as due to the resolution of EDX measurements the analysis cannot be confined to elements in the layer only.

Beneath the MML, cracks were observed in the cross-sections of all discs investigated (Fig. 7b–9b). They were best visible for pairing I (DI, Fig. 7b), where fractured tungsten carbides could be identified in a zone of ~15 µm beneath the surface. For Pairing II (DII, Fig. 8b) this heavily affected zone, where cracks in W_xC particles could be observed, was less pronounced and only ~10 µm thick. For DIII, with the smallest W_xC particles, cracked particles and cracks could only be identified up to ~2 µm beneath the surface (Fig. 9b). This decreasing affected zone with decreasing particle size is probably due to higher bending stress occurring in larger particles when they are loaded. Further, these results show that although the stresses in the tribosystem are large enough to crack W_xC particles, the interface between binder phase and W_xC particles was strong enough to prevent pull-out of entire W_xC particles in any of the pairings investigated. Thus, the extent of the heavily affected zone underneath the surface decreased with decreasing particle size of the hard metal used for the discs, hence, the material became less prone to wear.

The surface coverage of the discs with MMLs was different for the three pairings. Whereas the patches on DI (Fig. 7a) were typically smaller than 100 µm, those on DII (Fig. 8a) were substantially larger, reaching several 100 µm. On DII, the majority of the tribolayer was smooth and only partially interrupted by small, shallow pits and plateaus of bulk material. The disc of Pairing III was almost entirely covered with a thin tribolayer. Apparently, the coverage is promoted by the finer microstructure of the disc, possibly larger W_xC grains in the other discs prevent an interconnection of transferred binder, which is the main content of the bottom layer in DIII's tribolayer.

The pin surfaces showed significantly less tribolayer coverage,

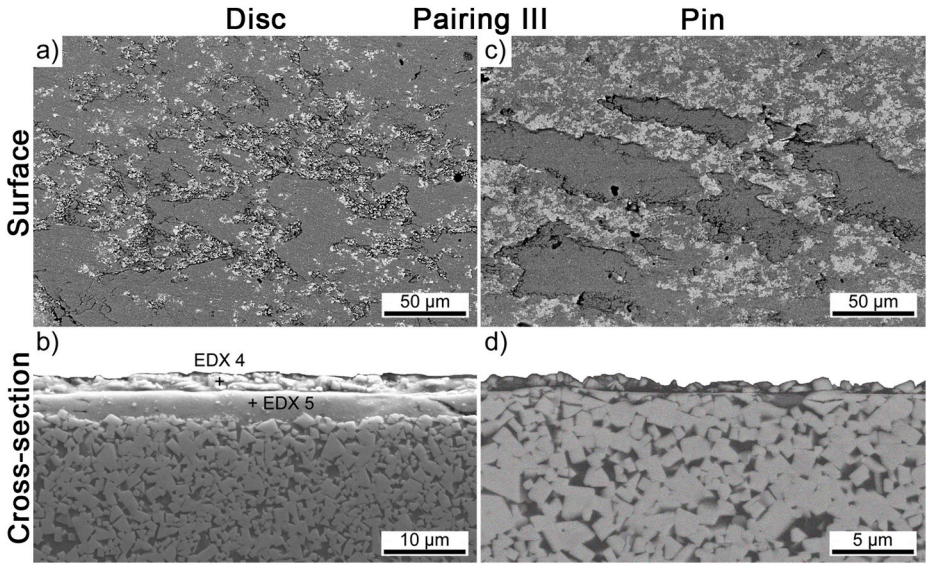

Fig. 9. SEM imaging of Pairing III: a) surface SEM-BSE of disc, b) cross-section SEM - SE of disc, c) surface SEM-BSE of pin, cross-section of pin, d) cross-section SEM - SE of pin.

Table 3
Results of the EDX measurements to Figs. 7–9 and 12.

[wt. %]	PI	DII	PII	DIII		DIII (PI-DIII)	
	EDX 1	EDX 2	EDX 3	EDX 4	EDX 5	EDX 6	EDX 7
C	1.94	2.52	2.61	34.17	8.40	7.90	8.60
O	17.33	11.79	12.06	20.55	13.87	6.10	11.50
Co	10.80	12.62	6.81	5.86	10.91	12.80	8.70
Ni	–	–	2.67	–	–	–	
W	69.93	73.08	75.85	39.42	66.82	73.1	71.10

leading to the conclusion that the permanent contact of the pin with the disc impaired a full coverage and facilitated constant removal of the tribolayer. The tribolayer coverage of the individual pin surfaces was quantified via image analysis of the SEM top-views and revealed ~15%, 25%, and 45% coverage for Pairing I, II, and III, respectively. Figs. 7c–9c show the most pronounced tribolayer patches. These patches were similar to the layers on the discs regarding their chemical composition, as shown on spot EDX 1 in Table 3: they consisted of binder, oxidised binder and broken W_xC particles. Pairing II offered the possibility to clarify the origin of these patches, as the pins and the disc contained chemically different binders: DII featured the commonly used Co-binder, the PII was made with Ni-binder. EDX 3 showed a distinct Co-content (even higher than the Ni-content), indicating significant material transfer from the disc to the pin.

Detailed investigations of the cross-sections of the pins (Figs. 7d–9d) showed that the inter-particle distance in the near-surface regions were substantially reduced during the sliding contact: the W_xC particles were now almost touching each other, suggesting that the binder phase was pressed out from the first ~2 µm below the surface. However, cracking of the particles was hardly observed in the pins compared to the discs, probably because the broken particles were preferably removed.

Based on these investigations of the discs and pins, it can be concluded that the tribolayers were composed of fragmented W_xC particles, binder phase and oxidised binder. As the size of the fragmented particles was influenced by the initial W_xC particle size, the tribolayer on the surface of disc DIII had the finest particles and highest amount of binder, both more homogeneously distributed than the other tribolayers. Therefore, the tribolayer on DIII was extremely smooth and able to almost entirely cover and protect the disc. In contrast, the tribolayers formed on Pairing I and II were composed of larger W_xC fragments and covered the surface to a lesser extent. These results are also represented by the surface topography as explained in the next section.

3.5. Topography evaluation

Surface sections of 0.5 × 0.5 mm in the centre of the wear track were chosen for both the discs and the pin samples for detailed topography measurements. The results are presented by a colour map in Fig. 10a–c for the discs and Fig. 10d–f for the pins. The colour code from blue to red covers a topology from −4 to +4 µm. This overview clearly shows that PI and especially PII were much smoother than their corresponding discs, they were worn uniformly and formed tribolayers did not roughen the surface significantly.

The surface roughness of the discs decreased from I to II to III (corresponding to their decreasing particle size and increasing hardness). However, the surface roughness of the pins showed the opposite trend and increased from I to II to III. Apparently, the higher the similarity of the hard-metal pairings of discs and pins are, with respect to hardness and particle sizes, the more the wear volume was evenly distributed among both sliding partners.

3.6. Morphology of tribolayers

The carbides within the surface near regions of the hard metals were pressed closer together (especially at the pins, which are higher loaded than the discs) followed by localised plasticisation effects, similar to observations which made Larsen-Basse [44] already in 1985 for high-stress hard metal contacts. That the tribolayer was mainly formed on the discs and only partly on the pins could be clearly derived from cross-section analysis. For both parts, discs and pins, no failure of the interface between binder-phase and W_xC particles (which would also result in a significant W_xC particle pull-out behaviour) was observed. The high contact stresses during the tribocontact led to cracking of the W_xC particles underneath the contact surfaces, i.e. local normal pressures must far exceed the nominal contact pressure of 10.6 MPa. The depth of this subsurface zone (where cracked W_xC particles were observed) strongly depended on the original W_xC particle size of the hard metals. This depth was smallest for the hard metals with the smallest particle size (i.e., ~10 µm for DI, and only ~2 µm for DIII). Cracking of the W_xC particles in the subsurface zone may additionally be enhanced by the softening of the metallic matrix due to an increase in temperature caused by friction. In the measured temperature range,

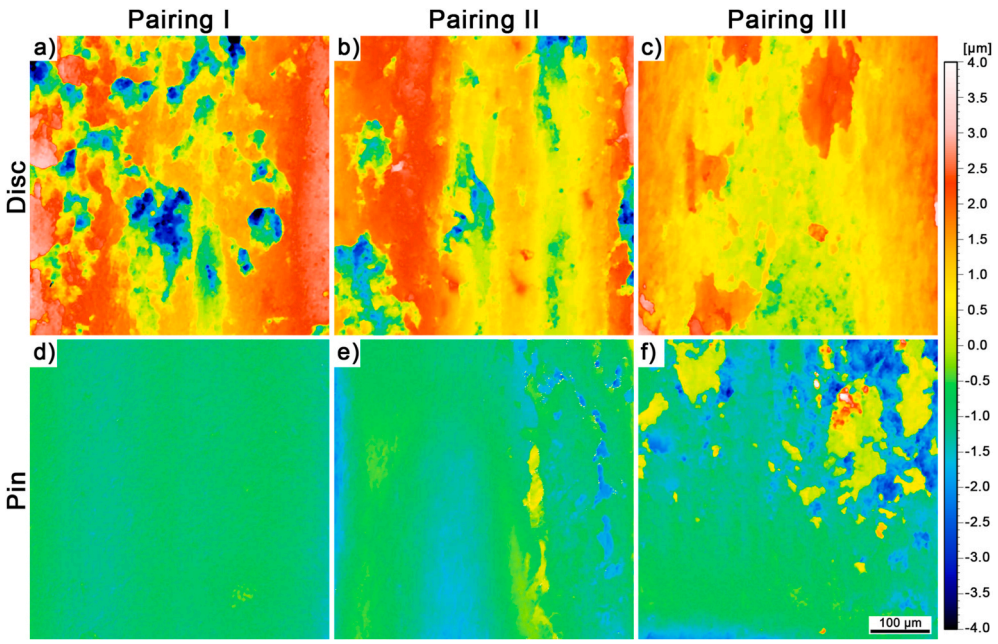

Fig. 10. Surface topographies of the tribo-pairings: a) DI, b) DII, c) DIII; d) PI, e) PII, f) PIII.

frictional heating will have little effect on the carbides in the disc, but primarily affect the binder [31], whose ability to carry the carbides will decrease and promote particle cracking.

Pirso et al. [17] and Saitu et al. [45] already found a strong correlation of wear resistance in dry sliding regime (hard metal against carbon steel) with W_xC particle size and free path length/increasing binder content between the carbides: larger W_xC grains reduced the wear resistance, while lower binder content increased the wear resistance. This relationship agrees to the findings in the current study, where the pairing with the smallest grain size is the most wear resistant. The formed tribolayer determines the wear resistance in this work, which was not studied in [45]. First indications of similar layers were reported, at high load conditions, in [17], but not analysed in detail. In this study, the initial W_xC particle size not only determined the depth of the subsurface damage zone, but also the homogeneity of the tribolayer at the contact surfaces. The larger the initial W_xC particle size, the larger the W_xC fragments within the tribolayer and MML. These W_xC fragments and their oxidation products have a low adhesion to the disc or pin, thus such tribolayers could exhibit a dynamic behaviour (rapid delamination and re-forming). Matikainen et al. [46] reported such behaviour for similar microstructures produced by thermal spraying. Therefore, the materials with large initial W_xC particle sizes showed the highest wear rates and CoF scattering, even in the steady-state region, which can be attributed to repeated, partial delamination of the tribolayer.

A homogeneous tribolayer and MML can evenly distribute the contact pressure, leading to lower peak values and a more evenly distributed stress field in the subsurface zone. The Pairings I and II – with the disc materials featuring the largest W_xC particle sizes – do not exhibit a continuous and homogenous tribolayer – there only patches of tribolayer cover the contact surfaces. In contrast, Pairing III exhibited a homogeneous tribolayer covering almost the entire disc surface. Pairing III showed the lowest wear rate, and the lowest CoF level of the tested pairings, although their tribolayer was the thinnest. Apparently, the homogeneous coverage of the tribolayer was more important than its thickness for low friction levels as well as low wear.

3.7. Additional sliding experiment

Based on the results presented above – that a small difference in particle size can already result in a beneficial tribolayer formation leading to a high wear resistance – additional sliding experiments were performed by pairing the material DIII with PI (which is not a commercially promoted pairing for check valves). These two materials had almost identical particle sizes (0.9 ± 0.5 µm for DIII and 1.0 ± 0.7 µm for PI) although the disc was slightly softer (1180 ± 19 HV30) than the pin (1370 ± 25 HV30). This is desirable for the application, as the more easily exchangeable part (shut-off ring) is supposed to wear first.

The CoF curve of this new pairing (PI-DIII) was similar to those obtained for Pairing I and II, with a steady state CoF value of 0.5–0.6. But the major advantage of this new pairing was the considerably reduced wear rate compared to the other pairings, see Fig. 11. The direct comparison with Pairing I and III highlights that with the new combination, the best of both worlds could be combined to entail low total wear. The pin wear (2.8×10^{-6} mm^3 N^{-1} m^{-1}) was almost identical to that of Pairing I and the disc wear (0.25×10^{-4} mm^3 N^{-1} m^{-1}) was only slightly larger than the very low disc wear value (0.21×10^{-4} mm^3 N^{-1} m^{-1}) observed for Pairing III.

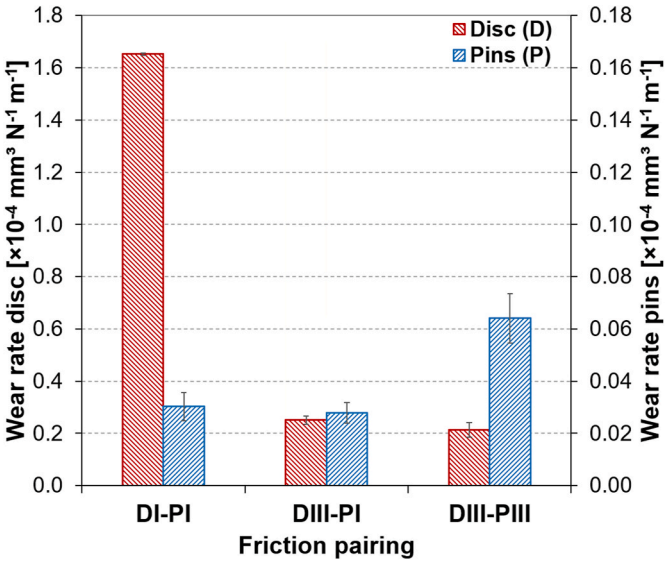

Fig. 11. Wear rates (rearranged) of additional Pairing DIII-PI compared to Pairings DI-PI and DIII-PIII.

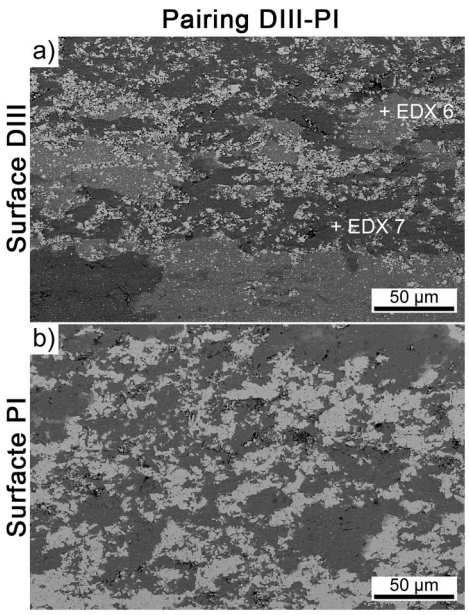

Fig. 12. SEM investigation of pairing DIII-PI: a) surface SEM-BSE of disc III, b) surface SEM-BSE of pin I.

SEM-BSE investigations of the wear tracks (Fig. 12) revealed a high tribolayer coverage on the disc (Fig. 12a). This tribolayer is composed of regions of oxidation products with lower O-content (appearing greyish in Fig. 12a; EDX 6 in Table 3) and oxidation products with higher O-content (dark grey appearance in Fig. 12a; EDX 7 in Table 3). Especially the higher regions with higher oxygen content were very similar to the beneficial tribolayer formed on DIII (EDX 5 in Table 3). We envision, that the regions with lower O-content are early stages of the tribolayer, either thinner or less oxidised Co. Nevertheless, in total the tribolayer formed on this new pairing was almost as effective as the tribolayer on pairing PIII-DIII.

PI showed a nearly identical wear rate when worn against DIII or DI, as shown above. This is thought to be based on the effective tribolayer formed on PI when in contact against DIII, which is obviously independent from the counterbody change from DI to DIII.

3.8. Beneficial tribolayers and their occurrence in other applications

Beneficial and protective tribolayer and MML formation are known from some heavy wear applications, where a mixture of carbides, metal and oxides offer an effective wear protection. For example, during high temperature sliding contacts of steels, a formation of a tribolayer composed of oxidation products proved to be very effective for wear protection in [47]. Third body phenomena, like in abrasion processes, or in our case through broken W_xC particles can lead to the formation of protective tribolayers [36–38]. showed that the embedment of externally added abrasive particles in MMLs increases their wear resistance and even protects materials initially containing no hard phases. Oxides can contribute to the wear resistance, as they may also reduce adhesion between metallic counterbodies [42]. showed that at certain conditions of hard metal in a dry contact a tribolayer can be formed even without a metallic counterbody, i.e. all tribolayer constituents origin from the first body (and environmental conditions).

To summarize, in our contact situation a tribolayer or MML consisting of rather small W_xC fragments and relatively high amounts of binder phase in addition to oxidised binder covers the surfaces homogeneously and is thus beneficial to protect the hard material partners in contact. Thereby, contact pressures can be evenly distributed, reducing peak loads and avoiding further hard metal damage by hindering cracking of W_xC.

3.9. Tribolayer formation model

Based on the obtained results, the authors envision that the wear behaviour and tribolayer formation during hard metal – hard metal sliding contact can be described by the following qualitative model, which is schematically given in Fig. 13:

a) Hard metal - hard metal asperity contact entailing extremely high contact pressures occur, which are able to break individual W_xC particles. Sliding at high pressures is accompanied by considerable frictional heating.

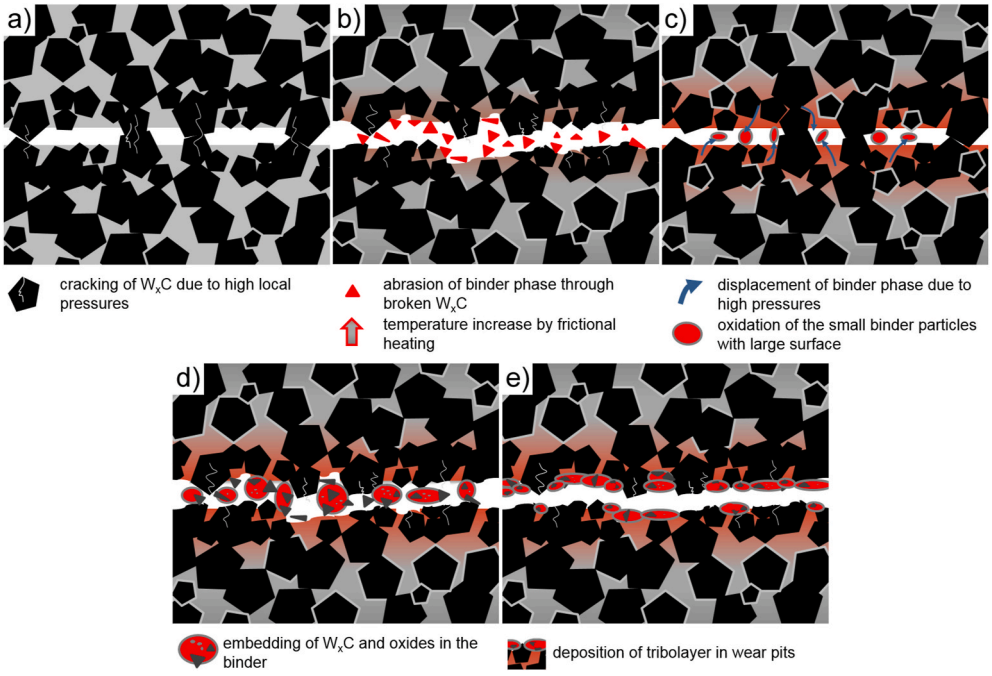

Fig. 13. Schematic of possible tribolayer formation in dry sliding hard metal - hard metal contact.

b) Small broken hard metal particles move freely between the counteracting bodies as third bodies. In this abrasive wear regime, the small, highly angular particles are able to abrade the binder phase between the W_xC particles. The temperature increase promotes binder phase softening.
c) Due to high contact loads and increases in temperature, the binder phase is pressed out from regions between the W_xC particles (especially in the pin/flights, as this cannot cool down during operation). The newly generated binder surfaces easily oxidise at the higher temperatures prevailing in the sliding surface.
d) Due to the high temperatures in the tribocontact, the binder is thermally softened and third bodies, i.e. the broken W_xC particles and oxides, can be easily embedded.
e) The tribolayer gets pressed in wear pits on the surface and cools down due to the increased contact area to the bulk material. Delamination and reformation of the tribolayer is a steady process in the sliding tribocontact.

The beneficial effect of a tribolayer is, at a minimum, based on the better load distribution (e.g., the local contact pressures significantly decrease if the tribolayer homogeneously covers both areas in contact and reduces the roughness) and the reduced adhesion (e.g., metal-metal contact of binder phases is reduced by the tribolayer, which consists partly of carbides and oxides).

4. Conclusions

This study focuses on the severe wear process of dry hard metal - hard metal contact experienced by check valves in injection moulding when the lubricating plastic mould film fails. Three material pairings were tested in a three-pins-on-disc set-up and the major findings of this work were:

- Tribolayer formation – the in-situ evolution of an effective wear protective layer – occurs in all pairings: The tribolayers consist of broken W_xC particles, binder, oxides and transferred material from the counterbody.
- Wear is dominated by breaking of the W_xC particles. First, the largest carbides in the microstructure crack, but are not pulled out of the matrix. Broken, free moving fragments are embedded in the binder, forming the tribolayer. Wear happens via delamination of this tribolayer, leaving shallow – but rough – dimples behind.
- Tribolayers with more binder and smaller W_xC or oxide fragments are smoother, resulting in lower wear losses. A tribolayer covering a large part of the surface is thought to distribute the load more evenly, reducing wear further.
- The coarse-grained pairings showed a patchy tribolayer structure with less total coverage, while the fine-grained pairings showed an almost surface-covering tribolayer. Thus, the finer the W_xC grain size, the lower the wear rate in the present study.

Based on the results we can conclude that the wear of dry sliding check valves can be significantly reduced by optimising the material pairings, thus giving the possibility to enhance the lifetime of dry sliding hard metal - hard metal contacts significantly.

Declaration of competing interest

The authors declare the following financial interests/personal relationships which may be considered as potential competing interests: The authors declare no conflict of interest.

Acknowledgements

This work was funded by the “Austrian COMET Program” (project InTribology, no. 872176) via the Austrian Research Promotion Agency (FFG) and the federal states of Niederösterreich and Vorarlberg and has been carried out within the “Excellence Centre of Tribology” (AC2T research GmbH). The authors acknowledge TU Wien Bibliothek for financial support through its Open Access Funding Programme. The authors are also thankful for the tribotesting of the individual material combinations, performed by Thomas Lebersorger and Lukas Spiller, and for fruitful discussions with Ewald Badisch and Claudia Lenauer.

References

[1] J. Iwko, R. Steller, R. Wróblewski, Experimentally verified mathematical model of polymer plasticization process in injection molding, Polymers 10 (2018) 968–995.
[2] A.L. Kelly, W. Woodhead, P.D. Coates, Comparison of injection molding machine performance, Polym. Eng. Sci. 45 (2005) 857–865.
[3] A. Blutmager, T. Spahn, M. Varga, W. Friesenbichler, H. Riedl, P.H. Mayrhofer, Processing fibre reinforced polymers: specific wear phenomena caused by filler materials, Polym. Eng. Sci. 60 (2020) 78–85.
[4] S. Hua, S. Zhang, W. Cao, Y. Wang, C. Shao, C. Liu, B. Dong, C. Shen, Simulation of jetting in injection molding using a finite volume method, Polymers 8 (2016) 172–182.
[5] J. Iwko, R. Steller, R. Wróblewski, Experimentally verified mathematical Model of polymer plasticization process in injection molding, Polymers 10 (2018) 968–995.
[6] A. Blutmager, M. Varga, T. Schmidt, A. Pock, W. Friesenbichler, Abrasive/erosive wear on MMCs in plastic molds as a function of volumetric flow rates and glass fiber distribution, Polym. Eng. Sci. 59 (2019) 302–311.
[7] F. Johannaber, W. Michaeli, Handbuch Spritzgießen, Hanser, 2001.
[8] G. Mennig, M. Lake, Verschleißminimierung in der Kunststoffverarbeitung, Hanser, 2008.
[9] C.J. Gornik, Neue Erkenntnisse zur Plastifiziereinheit von Spritzgießmaschinen basierend auf experimentellen Untersuchungen, Dissertation Montanuniversität Leoben, 2007.
[10] A. Blutmager, M. Varga, P.H. Mayrhofer, W. Friesenbichler, Friction and wear behaviour in dry sliding of hard metals, in: Proceedings of 6th World Tribology Congress, 2017.
[11] Federico Bosio, Emilio Bassini, Cristina Gabriela Oñate Salazar, Daniele Ugues, Daniele Peila, The influence of microstructure on abrasive wear resistance of selected cemented carbide grades operating as cutting tools in dry and foam conditioned soil, Wear 394–395 (2018) 203–216.
[12] S. Novak, M. Soković, B. Navinšek, M. Komac, B. Praček, On the wear of TiN (PVD) coated cermet cutting tools, Vacuum 48 (1997) 107–112.
[13] L. Toller, S. Jacobson, S. Norgren, Life time of cemented carbide inserts with Ni-Fe binder in steel turning, Wear 376–377 (2017) 1822–1829.
[14] J. Lorentzon, N. Järvstråt, Modelling tool wear in cemented-carbide machining alloy 718, Int. J. Mach. Tool Manufact. 48 (2008) 1072–1080.
[15] J.B.J.W. Hegeman, J.ThM. De Hosson, G. de With, Grinding of WC–Co hardmetals, Wear 248 (2001) 187–196.
[16] F.A. Almeida, A.J.S. Fernandes, F.J. Oliveira, R.F. Silva, Semi-orthogonal turning of hardmetal with CVD diamond and PCD inserts at different cutting angles, Vacuum 83 (2009) 1218–1223.
[17] J. Pirso, S. Letunovitš, M. Viljus, Friction and wear behaviour of cemented carbides, Wear 257 (2004) 257–265.
[18] J.A.R. Wesmann, N. Espallargas, Effect of atmosphere, temperature and carbide size on the sliding friction of self-mated HVOF WC-CoCr contacts, Tribol. Int. 101 (2016) 301–313.
[19] G.S. Upadhyaya, Cemented Tungsten Carbides : Production, Properties, and Testing, Noyes Publications, 1998.
[20] S.S. Ponomarev, A.V. Shatov, A.A. Mikhailov, S.A. Firstov, Mechanisms for the degradation of strength and wear-resistance of WC based cemented carbides due to faster cooling, Int. J. Refract. Metals Hard Mater. 49 (2015) 161–169.
[21] H. Saito, A. Iwabuchi, T. Shimizu, Effects of Co content and WC grain size on wear of WC cemented carbide, Wear 261 (2006) 126–132.
[22] M. Aristizabal, L.C. Ardila, F. Veiga, M. Arizmendi, J. Fernandez, J.M. Sánchez, Comparison of the friction and wear behaviour of WC-Ni-Co-Cr and WC-Co hardmetals in contact with steel at high temperatures, Wear 280–281 (2012) 15–21.
[23] A.J. Gant, M.G. Gee, Abrasion of tungsten carbide hardmetals using hard counterfaces, Int. J. Refract. Metals Hard Mater. 24 (2006) 189–198.
[24] Sunny Zafar, Apurbba Kumar Sharma, Microstructure and wear performance of heat treated WC-12Co microwave clad, Vacuum 131 (2016) 213–222.
[25] R. Polak, S. Ilo, E. Badisch, Relation between inter-particle distance (L_{IPD}) and abrasion in multiphase matrix-carbide materials, Tribol. Lett. 33 (2009) 29–35.
[26] K.H. Zum Gahr, Microstructure and Wear of Materials, 10, Elsevier Science Publishers B.V., Siegen, 1987.
[27] E. Badisch, S. Ilo, R. Polak, Multivariable modeling of impact-abrasion wear rates in metal matrix-carbide composite materials, Tribol. Lett. 36/1 (2009) 55–62.
[28] K. Bonny, P. De Baets, Y. Perez, J. Vleugels, B. Lauwers, B. de Patrick, J. Vleugels, S. Huang, B. Lauwers, Friction and wear characteristics of WC-Co cemented carbides in dry reciprocating sliding contact, Tribol. Trans. 52 (2010) 481–491.
[29] S. Hernandez, J. Hardell, H. Winkelmann, M.R. Ripoll, B. Prakash, Influence of temperature on abrasive wear of boron steel and hot forming tool steels, Wear 338–339 (2015) 27–35.
[30] H. Engqvist, H. Högberg, G.A. Botton, S. Ederyd, N. Axén, Tribofilm formation on cemented carbides in dry sliding conformal contact, Wear 239 (2000) 219–228.

[31] H. Berns, Microstructural properties of wear-resistant alloys, Wear 181–183 (1995) 271–279.
[32] A. Zikin, I. Sotiraq, K. Priit, I. Hussainova, C. Katsich, E. Badisch, Plasma transferred arc (PTA) hardfacing of recycled hardmetal reinforced nickel-matrix surface composites, Mater. Sci. 18/1 (2012) 12–17.
[33] H. Torres, M. Varga, M.R. Ripoll, High temperature hardness of steels and iron-based alloys, Mater. Sci. Eng. 671 (2016) 170–181.
[34] H. Rojacz, M. Varga, H. Kerber, H. Winkelmann, Processing and wear of cast MMCs with cemented carbide scrap, J. Mater. Process. Technol. 214 (2014) 1285–1292.
[35] H. Winkelmann, E. Badisch, M. Varga, H. Danninger, Wear mechanisms at high temperatures. part 3: changes of the wear mechanism in the continuous impact abrasion test with increasing testing temperature, Tribol. Lett. 37 (2010) 419–429.
[36] M. Antonov, I. Hussainova, Cermets surface transformation under erosive and abrasive wear, Tribol. Int. 43/8 (2010) 1566–1575.
[37] M. Antonov, I. Hussainova, J. Pirso, O. Volobueva, Assessment of mechanically mixed layer developed during high temperature erosion of cermets, Wear 263 (2007) 878–886.
[38] M. Varga, High temperature abrasive wear of metallic materials, Wear 376–377 (2017) 443–451.
[39] A. Nisar, K. Balani, Role of interfaces on multi-length scale wear mechanics of TaC-based composites, Adv. Eng. Mater. 19/5 (2017).
[40] V. Jankauskas, M. Antonov, V. Varnauskas, R. Skirkus, D. Goljandin, Effect of WC grain size and content on low stress abrasive wear of manual arc welded hardfacings with low-carbon or stainless steel matrix, Wear 328–329 (2015) 378–390.
[41] S.F. Murray, P. Lewis, Evaluation of rolling contact in the range of 550°F to 1000°F, General Electric, Feb. 7, 1958.
[42] C. Chen, Z. Guo, S. Li, Y. Xiao, B. Chai, J. Liu, Microstructure and properties of WC-17Co cermets prepared using different processing routes, Ceram. Int. (2019) in press.
[43] J. Prost, G. Boidi, T. Lebersorger, M. Varga, G. Vorlaufer, Comprehensive Review of Tribometer Dynamics – Cycle-Based Data Analysis and Visualization, accepted for publication in Friction, 2021.
[44] J. Larsen-Basse, Binder extrusion in sliding wear of WC-Co alloys, Wear 105 (1985) 247–256.
[45] H. Saito, A. Iwabuchi, T. Shimizu, Effects of Co content and WC grain size on wear of WC cemented carbide, Wear 261 (2006) 126–132.
[46] V. Matikainen, G. Bolelli, H. Koivuluoto, P. Sassatelli, L. Lusvarghi, P. Vuoristo, Sliding wear behaviour of HVOF and HVAF sprayed Cr_3C_2-based coatings, Wear 388–389 (2017) 57–71.
[47] H. Torres, M. Varga, F. Widder, U. Cihak-Bayr, O. Viskovic, M. Rodríguez Ripoll, Experimental simulation of high temperature sliding contact of hot rolled steel, Tribol. Int. 93 (2016) 745–754.